Site-specific and time-dependent activation of the endocannabinoid system after transection of long-range projections

Sonja Kallendrusch, Constance Hobusch, Angela Ehrlich, Simone Ziebell, Natsuo Ueda, Gerd Geisslinger, Marco Koch, Faramarz Dehghani

PLoS one

Site-Specific and Time-Dependent Activation of the Endocannabinoid System after Transection of Long-Range Projections

Sonja Kallendrusch[1,2], Constance Hobusch[1], Angela Ehrlich[1], Simone Ziebell[3], Natsuo Ueda[4], Gerd Geisslinger[3], Marco Koch[1], Faramarz Dehghani[1]*

1 Institute for Anatomy, Leipzig University, Leipzig, Germany, 2 Lipid Signaling Forschungszentrum, Frankfurt, Germany, 3 Institute for Pharmacology, Goethe University, Frankfurt, Germany, 4 Department of Biochemistry, Kagawa University, School of Medicine, Kagawa, Japan

Abstract

Background: After focal neuronal injury the endocannabinioid system becomes activated and protects or harms neurons depending on cannabinoid derivates and receptor subtypes. Endocannabinoids (eCBs) play a central role in controlling local responses and influencing neural plasticity and survival. However, little is known about the functional relevance of eCBs in long-range projection damage as observed in stroke or spinal cord injury (SCI).

Methods: In rat organotypic entorhino-hippocampal slice cultures (OHSC) as a relevant and suitable model for investigating projection fibers in the CNS we performed perforant pathway transection (PPT) and subsequently analyzed the spatial and temporal dynamics of eCB levels. This approach allows proper distinction of responses in originating neurons (entorhinal cortex), areas of deafferentiation/anterograde axonal degeneration (dentate gyrus) and putative changes in more distant but synaptically connected subfields (cornu ammonis (CA) 1 region).

Results: Using LC-MS/MS, we measured a strong increase in arachidonoylethanolamide (AEA), oleoylethanolamide (OEA) and palmitoylethanolamide (PEA) levels in the denervation zone (dentate gyrus) 24 hours post lesion (hpl), whereas entorhinal cortex and CA1 region exhibited little if any changes. NAPE-PLD, responsible for biosynthesis of eCBs, was increased early, whereas FAAH, a catabolizing enzyme, was up-regulated 48hpl.

Conclusion: Neuronal damage as assessed by transection of long-range projections apparently provides a strong time-dependent and area-confined signal for de novo synthesis of eCB, presumably to restrict neuronal damage. The present data underlines the importance of activation of the eCB system in CNS pathologies and identifies a novel site-specific intrinsic regulation of eCBs after long-range projection damage.

Introduction

Functional deficits of the central nervous system (CNS) are provoked by direct or delayed tissue damage. Lesions of long-range projections as it occurs in spinal cord injury (SCI), traumatic brain injury (TBI) or stroke often results in severe neurological impairment finally leading to persistent clinical and social disabilities for the patients [1]. At cellular level, CNS injury provokes primary and secondary processes that involve biochemical cascades occurring from minutes to weeks [2]. Earlier experimental studies identified different regulatory, inflammatory or immunological factors that were closely associated with secondary damage such as lipid degradation, altered neurotransmitter release and receptor function [3,4]. Neuronal cell death, reactive astrogliosis, microglia proliferation and activation are further consequences [5]. Research within the last two decades revealed that the endocannabinoid (eCB) system, among many

different signaling pathways reflects a major modulating signaling machinery of excitotoxicity by influencing neuronal damage either in a destructive or protective way [6].The eCB system includes a diverse group of long-chain fatty acids, the eCBs, acting on two cloned cannabinoid receptors [7], namely the cannabinoid receptor type 1 (CB_1) and type 2 (CB_2) and several not yet cloned cannabinoid receptors [8,9]. Well characterized eCBs like arachidonoylethanolamide (AEA) or 2-arachidonoylglycerol (2-AG) are partial or full agonists at CB_1 and CB_2 [10,11]. However, some structurally-related fatty acids like oleoylethanolamide (OEA) and palmitoylethanolamide (PEA) both showing biological effects similar to endocannabinoids are considered as members of the eCB family even without binding to CB_1 and CB_2, respectively [12].

Chemically defined as N-acylethanolamines (NEA), AEA, OEA and PEA are synthesized on demand from membrane glycerophospholipids by highly specific enzymes. N-acyl phosphatidyletha-

nolamine-selective phospholipase D (NAPE-PLD) reflects the rate limiting enzyme for biosynthesis of all three above mentioned NEA [13]. Generally, NEA have a short half-time and are selectively degraded. Fatty acid amide hydrolase (FAAH) is the best characterized enzyme that catabolizes NEA with the highest affinity for AEA [14,15]. However, N-acyletanolamide-hydrolyzing acid amidase (NAAA) was recently discovered as a novel NAE-hydrolyzing enzyme with a preference for PEA [16].

The broad spectrum of eCB-mediated biological actions involves analgesia and anti-inflammation in the central nervous system as well as in peripheral tissues. However, very little is known about the time course of induction and precise regulation of the eCB system after transection of long-range projections in the origin and targeted brain areas. These long-range projections connecting developmentally distinct areas of the CNS are often harmed in various insults, like SCI, TBI and stroke. Organotypic entorhino-hippocampal slice cultures (OHSC) allow the investigation of such long-range projections since projection fibers (perforant pathway) originating from EC neurons terminate at the outer molecular layer of the DG and thus connects two evolutionary distinct brain regions. The deafferentiation of the dentate gyrus by perforant pathway transection is a powerful tool to study cellular and inflammatory responses not only at the lesion site but also on anterograde projection areas [17,18,19,20,21].

In the present study we thus assumed an involvement of the eCB system and a possible neuroprotective role of its members not only at origin areas but also on neuronal populations localized in distant regions. The regulation of AEA, OEA and PEA levels and their main synthesizing and catabolizing enzymes were studied up to 72 hours after PPT. Moreover, the respective cell type being responsible for eCB production, release and/or catabolism, namely neurons, microglia or astrocytes were determined.

Methods

Ethics statement

All animal experiments have been approved by the ethics committees of the German federal states of Hessen or Saxonia and were performed in accordance with the Policy on Ethics and the Policy on the Use of Animals in Neuroscience Research as approved by the European Communities Council Directive (89/609/EEC) amended by the directive 2010/63/EU of European Parliament and of the Council of the European Union on the protection of animals used for scientific purposes.

Organotypic Entorhino-Hippocampal Slice Cultures (OHSC)

OHSC were prepared from 8-day old Wistar rats. Animals were decapitated and the brains were dissected under aseptic conditions [20]. After removal of the frontal lobe and the cerebellum, the brains were placed in 4°C minimal essential medium (MEM; Gibco BRL Life Technologies, Eggenstein, Germany) containing 1% (v/v) glutamine (Gibco). A sliding vibratome (Leica VT 1000 5, Leica Microsystems AG, Wetzlar, Germany) was used to cut the brain horizontally in 350 µm-thick slices. The hippocampus was dissected and immediately placed on cell culture inserts (pore size 0.4 µm; Millipore, Schwalbach/Ts., Germany) and were cultured in 6-well culture dishes (Falcon, BD Biosciences Discovery Labware, Bedford, MA) containing 1 ml culture medium (50% (v/v) MEM, 25% (v/v) Hanks' balanced salt solution (HBSS, Gibco), 25% (v/v) normal horse serum (NHS, Gibco), 2% (v/v) glutamine, 1.2 mg/ml glucose (Braun, Melsungen, Germany), 0.1 mg/ml streptomycin (Sigma-Aldrich, Deisenhofen, Germany), 100 µg/ml penicillin (Sigma-Aldrich), 0.8 µg/ml ascorbic acid

(Sigma-Aldrich) and 1 µg/ml insulin (Boehringer, Mannheim, Germany; pH 7.4)) per well. OHSC were cultured at 35°C in a fully-humidified atmosphere with 5% (v/v) CO_2. The culture medium was changed every second day.

Primary cell cultures

Primary cultures of hippocampal neurons were prepared using a modified method originally described by Brewer and colleagues [22]. Briefly, brains of P0 Wistar rats were removed and placed into a solution of ice-cold HBSS. The hippocampi were dissected and placed in Neurobasal Medium (Gibco) containing BSA (Sigma-Aldrich) and papain (1 mg/ml, Sigma-Aldrich) for 20 min at 37°C. Then neurons were isolated by tissue dissociation using Pasteur pipette, centrifuged for 10 min (45 g) and plated onto poly-L-lysine-coated coverslips. Cells were maintained in Neurobasal medium supplemented with B-27 (Gibco), GlutaMAX (Gibco) and penicillin/streptomycin at 37°C in a humidified atmosphere with 5% (v/v) CO_2 for 2 weeks.

Primary microglial and astrocyte cell cultures were isolated from cerebral cortices of P1 neonatal Wistar rats. After removal of the meninges, cerebral cortices were dissociated in Ca^{2+}/Mg^{2+}-free HBSS, containing trypsin (4 mg/ml, Boehringer) and DNAse (0.5 mg/ml, Worthington, Bedford, MA, USA). Cells were plated into poly-L-lysine (Sigma-Aldrich) coated 75 cm^2 tissue culture flasks (Falcon) containing DMEM (Gibco) supplemented with 4.5 g/l glucose (Gibco) and 10% (v/v) fetal bovine serum (FBS, Gibco), 1% (v/v) glutamine, 100 µg/ml penicillin and 100 µg/ml streptomycin.

Microglia was isolated from the astrocytic monolayer and incubated with control medium (DMEM supplemented with 2% (v/v) FBS, 1% (v/v) glutamine and 1% (v/v) penicillin/streptomycin). One day prior to all experiments, primary cultures of microglia and astrocytes were transferred into 24-well dishes coated with poly-L-lysine.
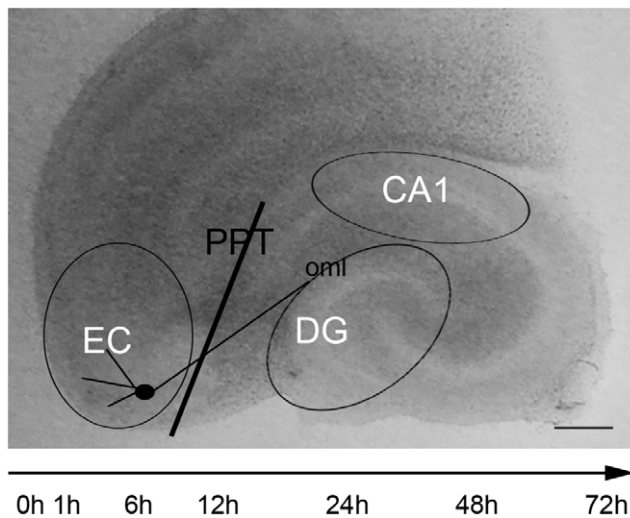
Perforant Pathway Transection (PPT)

The PPT was mechanically set on day 6 in vitro (div) by use of a disposable ophthalmic scalpel equipped with a stainless steel blade (Feather, Osaka, Japan). Under a binocular (Zeiss, Jena, Germany), PPT was performed within OHSC through the perforant pathway following the sulcus between the hippocampus and the entorhinal cortex (EC) [23]. The EC, the dentate gyrus (DG) and the cornu ammonis 1 (CA1) region were dissected 0, 1, 6, 12, 24, 48 or 72 hours post lesion (hpl; Fig. 1).

Neuronal damage

To analyze neuronal cell death, the medium of some OHSC was supplemented with 5 µg/ml propidium iodide (PI) 2 hours (h) prior to fixation with 4% (w/v) paraformaldehyde (Sigma-Aldrich) in 0.1 M phosphate buffer (PB). After fixation for at least 4 h, the cultures were washed twice with PB and embedded with Dako fluorescent mounting medium (Dako Diagnostika GmbH, Hamburg, Germany) and analyzed by a Zeiss LSM 510 Meta confocal laser scanning system (Zeiss, Göttingen, Germany). ImageJ software (U.S. National Institutes of Health, http://rsb.info.nih.gov/ij/download.html) was used for counting degenerating PI positive neuronal nuclei in the different EC, DG and CA1 regions.

LC-MS/MS

Tissues of 3 OHSC were pooled and immediately shock frozen in liquid nitrogen and stored at −80°C. Homogenization was performed on ice to prevent degradation of eCBs or internal standards. The extraction of eCBs was conducted with a 9:1 (v/v) ethylacetate/n-hexan solution [24]. The tissue was homogenized

Figure 1. Overview of the perforant pathway transection (PPT) in OHSC. The black line indicates the transection of the axons originating from layers II and III of entorhinal cortex (EC) and projecting to the outer molecular layer (oml) of the dentate gyrus (DG). The areas of EC, DG and cornu ammonis (CA)1 were dissected as visualized by the open black cycles. OHSC were kept in culture for 6 days before PPT was set and tissue of the highlighted areas was collected 1 h, 6 h, 12 h, 24 h, 48 h and 72 h post lesion. Bar = 500 µm.
doi:10.1371/journal.pone.0033537.g001

first in 70 µl ice cold H_2O in a mixer mill 400 (Retsch, Haan, Germany) for 90 seconds at 25 Hz. As a next step, 20 µl were taken away from the homogenates to quantify the protein amount of beta-actin by Western Blot analysis (see below). 50 µl of the tissue samples were again homogenized together with 25 µl of internal standards, 50 µl ethylacetate/n-hexan and 50 µl H_2O. After 3 minutes of centrifugation at 10,000 g, the organic phase was collected and the extraction procedure was repeated. The ethylacetate phases were evaporated under a gentle stream of nitrogen and assimilated in 25 µl acetonitril in glass vials. Finally, 10 µl were injected into the LC-MS/MS system (API, 5000, AB SCIEX, California, USA). For accuracy, quality standards were always extracted with the samples.

The reconstituted samples were analyzed for AEA, OEA and PEA. The respective deuterated AEA-d_8, OEA-d_2 and PEA-d_4 were used as internal standards. HPLC analysis was performed under gradient conditions using a Luna HST C18 (2) column (100 mm L×2 mm ID, 2.5 µm particle size; Phenomenex, Aschaffenburg, Germany). MS and MS/MS analyses were performed on an API 5000 triple quadrupole mass spectrometer with a Turbo V source (Applied Biosystems, Darmstadt, Germany) in the negative ion mode. Precursor-to-product ion transitions of m/z 346→259 for AEA, m/z 354→86 for AEA-d_8, m/z 324→86 for OEA, m/z 326→86 for OEA-d_2, m/z 298→268 for PEA and m/z 302→258 for PEA-d_4 were used for the multiple reaction monitoring (MRM) with a dwell time of 70 milliseconds. Concentrations of calibration standards, quality controls and unknowns were evaluated by Analyst software (version 1.4; Applied Biosystems). Variations in accuracy and intra-day and inter-day precision were <15% over the range of calibration. For each sample, endocannabinoid data was expressed in relation to the respective beta-actin level as obtained by Western Blot analysis (Image J 1.43, imagej.nih.gov/ij/download/) within the same sample. In each experiment protein extracts from controls and the corresponding PPT time matches were run onto the same gel to

ensure similar conditions for both groups. Endocannabinoid values were then normalized and values obtained from controls were set as 100%. Changes after PPT were described in relation to their corresponding time controls.

Western Blot analysis

For Western Blot analysis the tissue was collected and immediately stored in lysis buffer at −80°C. Protein extracts were obtained by sonication of tissues in lysis buffer containing 80 mM Tris, 70 mM SDS, 0,3 M Saccharose, 3 mM sodium orthovanadate and 0.5 mM phenylmethylsulfonyl fluoride (PMSF) at pH 7.4. Cell debris was removed by centrifugation for 10 min at 3000 g. Protein concentrations of the supernatants were determined by BCA test (Thermo Fisher Scientific, Rockford, USA). Equal protein amount of 5 µg were loaded onto a 12,5% (w/v) sodium dodecylsulfate–polyacrylamide gel. After gel electrophoresis, proteins were electrotransferred to nitrocellulose membranes. After blocking non-specific protein-binding sites for 1 h with 5% (w/v) milk (Carl Roth, Karlsruhe, Germany) or 5% (v/v) Roti-block solution (Carl Roth, Karlsruhe, Germany) in TBST, the membranes were incubated over-night with the respective following primary antibodies diluted in 5% (w/v) milk or 5% (v/v) Roti block in TBST: rabbit polyclonal antibody against human NAPE-PLD (diluted 1:1000; cat.-No 10305 (aa 6–20), Cayman Chemicals, Ann Arbor, MI, USA), rabbit polyclonal antibody against human FAAH (diluted 1:1000; cat.-No 101600 (aa 561–579), Cayman Chemicals), rabbit polyclonal antibody against rat NAAA (diluted 1:5000; developed by N. Ueda, Kagawa, Japan) [25], guinea pig polyclonal antibody against murine CB_1 (diluted 1:2000; cat.-No CB1-G P-Af530-1, Frontier Science, Hokkaido, Japan), PPAR alpha (diluted 1:1000; cat.-No PA1-822A, Thermo Scientific, Schwerte, Germany) and mouse monoclonal antibody directed against human beta-actin (diluted 1:40,000; cat.-No A1978, Sigma-Aldrich). The next day, membranes were washed three times with TBST for 10 min and the secondary horse radish peroxidase-conjugated antibodies (anti-rabbit, 1:1000; cat.-No PI 1000, Vektor laboratories, Burlingame, CA; anti-guinea pig 1:1000;cat.-No P0141, DAKO Diagnostika GmbH, Hamburg, Germany or anti-mouse IgG, 1:4000; cat.-No CP01, Millipore, Billerica, USA) were added for 1 h. Membranes were finally exposed to enhanced chemiluminescence (ECL detection system, Millipore) and the signal of bound antibody was visualized with radiographic films (Kodak, Stuttgart, Germany). Finally, semi-quantification of the immunoreactive bands was performed with ImageJ image analysis software.

Specificity tests for the antibodies used

The specificity of the antibodies was tested by preabsorption with the corresponding blocking peptides (NAPE-PLD, cat.-No 10303; FAAH, cat.-No 301600, Cayman Chemicals, respectively, NAAA, developed by Ueda's lab [25] and PPAR alpha, cat.-No PEP-025, Thermo Scientific). For preabsorption, each primary antibody was diluted in 5% (w/v) milk or 5% (v/v) Roti block in TBST and incubated with a five to ten-fold excess (by weight) of its blocking peptide for 1 h at room temperature with gentle shaking. Thereafter, the antibody-blocking peptide solution was applied to the Western Blot membranes and the subsequent procedures followed to the above described Western Blot protocol. The CB_1 antibody was tested on CB_1 (−/−) knock-out mice (kindly provided by Beat Lutz, Mainz, Germany, Fig. S1).

Immunohistochemistry

The OHSC were fixed with a 4% (w/v) paraformaldehyde solution in 0.1 M PB for at least 4 h. After fixation, OHSC were

washed in PB and incubated for at least 4 h in 15% (w/v) sucrose, followed by 30% (w/v) sucrose, respectively. Using a cryostat 3050 S (Leica, Wetzlar, Germany), the OHSC were sectioned (14 μm) and mounted on superfrost microscope slides (Thermo Scientific). To block unspecific binding sites sections were preincubated with normal goat serum for 30 min (1:20 in PBS/Triton) followed by incubation with primary antibodies for 16 h in PBS/Triton containing 0.5% (w/v) bovine serum albumin: NAPE-PLD (diluted 1:200), FAAH (diluted 1:200), NAAA (diluted 1:1000), CB_1 (diluted 1:100), PPAR alpha (diluted 1:1000). Binding of the primary antibodies was visualized by means of the ABC method with a biotin-conjugated anti-rabbit IgG (diluted 1:100; cat-No B7389 Sigma-Aldrich) as the secondary antibody, a horseradish peroxidase (HRP)-conjugated streptavidin complex (diluted 1:100; cat.-No E2886 Sigma-Aldrich) and 3, 3-diamino-benzidine as the chromogen. For immunocytochemical characterization of different cell populations within OHSC, the following primary antibodies were used: mouse monoclonal antibody against NeuN as a neuronal marker (diluted 1:200; cat.-No MAB377, Millipore), monoclonal mouse antibody against GFAP as a marker for astrocytes (diluted 1:200; cat.-No 556330, BD Pharmingen) and biotinylated isolectin B_4 (IB_4) as a marker for microglial cells (diluted 1:50; cat.-No FL-1201, Vector).

For triple-immunofluorescence staining, the primary antibodies against NAPE-PLD, FAAH, NAAA, CB_1 or PPAR alpha, were combined with FITC-conjugated isolectin B_4 and either with antibodies against NeuN or GFAP respectively. After incubation with primary antibodies for 16 h at room temperature, sections were washed three times with PBS followed by application of secondary antibodies Alexa fluor dye 568 (goat-anti rabbit IgG, 1:500, cat.-No A-11011, Invitrogen) and Alexa fluor dye 633 (goat anti-mouse IgG, 1:100, cat.-No A21050, Invitrogen, Karlsruhe, Germany) for 1 h. The preparations were finally coverslipped with Dako fluorescent mounting medium (Dako) and analyzed using a Zeiss LSM 510 Meta confocal laser scanning system.

Statistical analysis

Data from at least three independent experiments were expressed as mean values ($\pm$ standard error of the mean (SEM)). Data was statistically analyzed using ANOVA one way followed by Bonferroni posttests. Results with $p < 0.05$ were considered as significant. Analysis was conducted with Graph Pad Prism software 5 (GraphPad software, La Jolla, USA).

Results

Perforant Pathway transection does not increase neuronal cell death in the EC, DG or CA1 area

The determination of neuronal cell death by counting the numbers of propidium iodide (PI) positive nuclei revealed very few PI positive nuclei in the EC (CTL: 0hpl, 0.0; 1hpl, 0.0, 6hpl, 0.0; 12hpl 0.0; 24hpl, 1.7; 48hpl, 1.7; 72hpl, 0.0; PPT: 0hpl, 0.0; 1hpl, 0.3, 6hpl, 0.0; 12hpl, 0.0; 24hpl, 1.3; 48hpl, 1.7; 72hpl, 0.0). Similar findings were observed in the DG (CTL: 0hpl, 0.0; 1hpl, 0.3, 6hpl, 0.3; 12hpl, 0.3; 24hpl, 0.7; 48hpl, 1.0; 72hpl, 0.0; PPT: 0hpl, 0.3; 1hpl, 0.7, 6hpl, 0.0; 12hpl, 1.7; 24hpl, 1.7; 48hpl, 1.3; 72hpl, 2.0) and CA1 region (CTL: 0hpl, 0.0; 1hpl, 0.0, 6hpl, 0.0; 12hpl, 0.0; 24hpl, 0.0; 48hpl, 0.7; 72hpl, 0.0; PPT: 0hpl, 0.0; 1hpl, 0.3, 6hpl, 0.0; 12hpl, 0.0; 24hpl, 0.3; 48hpl, 0.7; 72hpl, 1.0). There was no significant change in the number of PI positive nuclei in investigated regions (EC, DG, CA1) at all time-points assessed ($p > 0.05$). No difference was found between controls and PPT slices ($p > 0.05$).

Endocannabinoid levels are regulated in a site specific and time dependent manner after PPT

Axonal dissection/dendritic denervation as induced by PPT led to a site-specific intrinsic upregulation of AEA, PEA and OEA levels in the DG (Fig. 2). The eCB levels of non lesioned controls (CTR) were set to 100% and the PPT data was expressed in relation to their time controls, respectively. Under control conditions (0hpl) following mean values for NEA were found in the areas investigated (AEA: EC, 0.015 ng/ml; DG, 0.010 ng/ml; CA1, 0.018 ng/ml; PEA: EC, 0.828 ng/ml; DG, 0.769 ng/ml; CA1, 1.475 ng/ml; OEA: EC, 0.094 ng/ml; DG, 0.076 ng/ml; CA1, 0.150 ng/ml, respectively). In the EC region no significant changes in NEA levels were observed after PPT. AEA levels in the EC remained at control levels (0hpl, 115%; 1hpl, 139%; 6hpl, 74%; 12hpl, 121%;24hpl, 112%; 48hpl, 82%; 72hpl, 79%; $p > 0.05$). Only at 1hpl a non significant elevation to 139% was observed (Fig. 2). At all time points investigated no significant change was detected for PEA (0hpl, 116%; 1hpl, 160%; 6hpl, 96%; 12hpl, 143%; 24hpl, 111%; 48hpl, 66%; 72hpl, 85%; $p > 0.05$, Fig. 2A) or OEA (0hpl, 106%; 1hpl, 157%; 6hpl, 86%; 12hpl, 130%; 24hpl, 121%; 48hpl, 75%; 72hpl, 99%; $p > 0.05$, Fig. 2).

In the DG AEA levels did not differ significantly from controls up to 12hpl (0hpl, 113%; 1hpl, 122%; 6hpl, 90%; 12hpl, 142%; $p > 0.05$). At 24hpl mean AEA levels were significantly increased compared to controls (24hpl, 261%; $p < 0.001$). Thereafter AEA levels declined (48hpl, 79%; $p > 0.05$) and were below the respective time control at 72hpl (72hpl, 82%; $p > 0.05$, Fig. 2B). PEA levels in the DG did not differ significantly from controls up to 6hpl (0hpl, 111%; 1hpl, 132%; 6hpl, 124%; $p > 0.05$, Fig. 2). At 12hpl, the PEA level were elevated (12hpl, 193%; $p < 0.05$) and reached the maximum at 24hpl (24hpl, 352%; $p < 0.001$). PEA levels then declined (48hpl, 56%; $p > 0.05$) and were reduced at 72hpl without reaching the significant threshold (72hpl, 76%; $p > 0.05$). OEA levels after PPT in the DG were comparable to control levels up to 12hpl, (0hpl, 101%; 1hpl, 129%; 6hpl, 131%; 12hpl, 143%; $p > 0.05$). At 24hpl OEA levels were maximal elevated (24hpl, 299%; $p < 0.001$). Thereafter OEA levels declined and were at 48hpl and 72hpl lowered compared to the respective time controls (48hpl, 61%; 72hpl, 81%; $p > 0.05$, Fig. 2).

In the CA1 region no significant changes were observed in AEA levels (0hpl, 114%; 1hpl, 107%; 6hpl, 113%; 12hpl, 66%; 24hpl, 90%; 48hpl, 59%; 72hpl, 106%; $p > 0.05$, Fig. 2). PEA levels remained close to the control levels until 12hpl (0hpl, 92%; 1hpl, 119%; 6hpl, 111%; 12hpl, 76%; $p > 0.05$, Fig. 2). At 24hpl (24hpl, 70%; $p > 0.05$) PEA levels were below control levels reaching the significant threshold at 48hpl (48hpl, 38%; 72hpl, 92%; $p < 0.05$). OEA levels in the CA1 region were comparable to the control levels up to 24hpl (0hpl, 84%; 1hpl, 112%; 6hpl, 132%; 12hpl, 77%; 24hpl, 64%; $p < 0.5$). At 48hpl the OEA levels decreased significantly compared to the control levels (48hpl, 44%; $p < 0.05$; 72hpl, 98%; $p > 0.5$, Fig. 2).

Differential regulation of enzymes and receptors of the eCB system after PPT

The site-specific and time-dependent changes in enzymes, namely NAPE-PLD, FAAH and NAAA as well as in receptors, namely CB_1 and PPAR alpha were analyzed by Western blot. The specificity of the used antibodies was tested by means of preabsorption (Fig. S1A). The CB1 antibody showed no signal in $CB_1^{-/-}$ animals (Fig. S1B). For densitometric analysis the PPT data was expressed relative to their time-controls, respectively and the control levels were set as 100%. No change in NAPE-PLD was
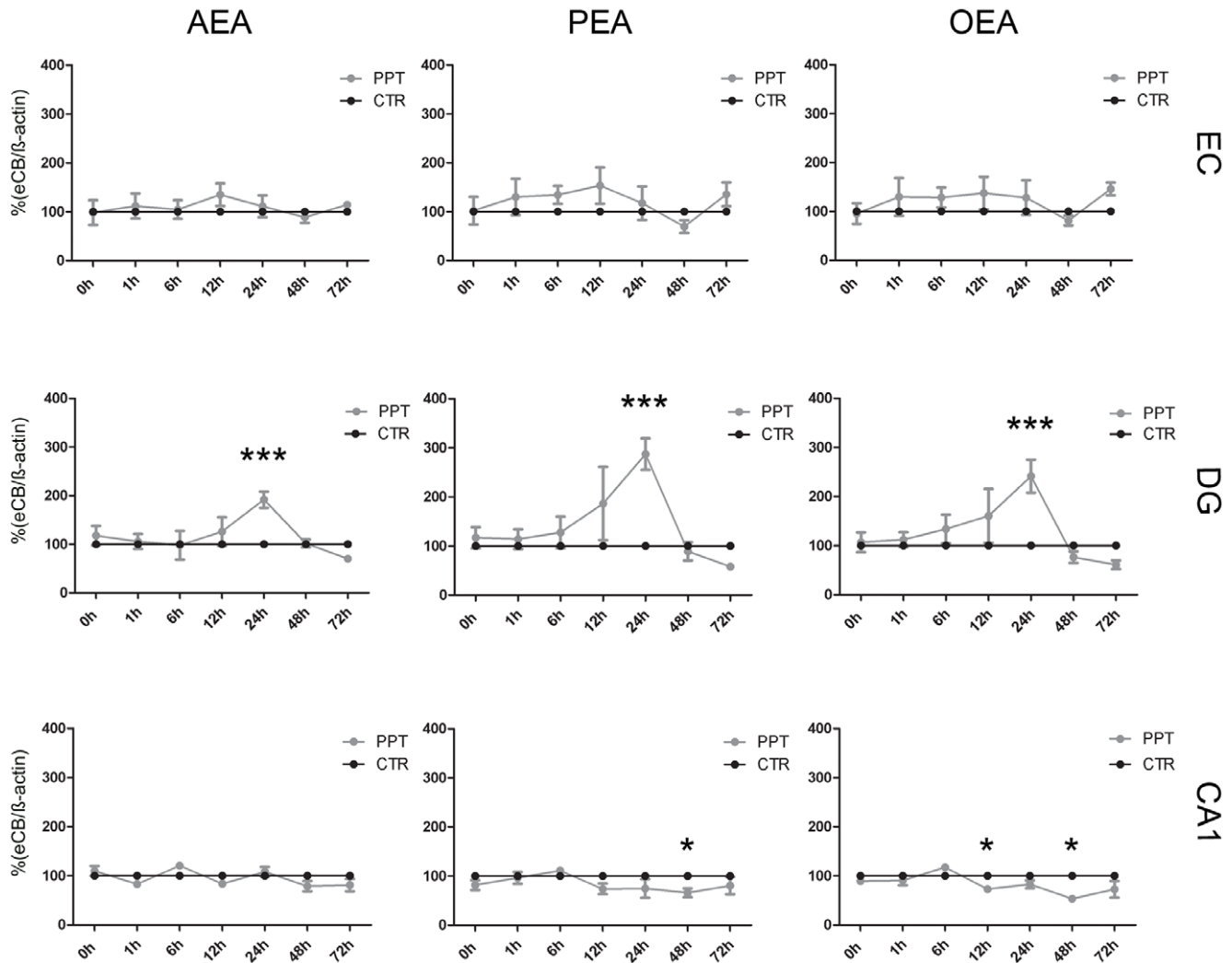
Figure 2. Endocannabinoid (eCB) levels in EC, DG and the CA1 region as normalized against ß-actin immunosignals. Control condition (CTR) of each time-point was set as 100% (black cycles). In EC AEA, PEA and OEA (gray circles, respectively) did not show any alteration in comparison to the respective CTR. In the DG, all investigated eCBs significantly increased 24hpl. In CA1, AEA did not differ from CTR after PPT. PEA showed a significant decrease 48hpl. OEA decreased at 12 and 48hpl. (n = 4, *p<0.05, ***p<0.001).
doi:10.1371/journal.pone.0033537.g002

detectable after axonal damage in the EC (0hpl, 98%; 1hpl, 114%; 6hpl, 105%; 12hpl, 114%; 24h, 102%; 48hpl, 111%; 72hpl, 119%; p>0.05; Fig. 3). Neither FAAH (0hpl, 83%; 1hpl, 115%; 6hpl, 104%; 12hpl, 98%; 24h, 88%; 48hpl, 97%; 72hpl, 90%; p>0.05; Fig. 3) nor NAAA (0hpl, 88%; 1hpl, 89%; 6hpl, 79%; 12hpl, 98%; 24h, 101%; 48hpl, 100%; 72hpl, 105%; p>0.05; Fig. S2) were significantly changed. After PPT CB_1 protein (0hpl, 86%; 1hpl, 94%; 6hpl, 129%; 12hpl, 92%; 24h, 101%; 48hpl, 108%; 72hpl, 132%; p>0.05; Fig. 3) was significantly increased after 1hpl (129%; p<0.05) and 72hpl (132%; p<0.05) in the EC only. PPAR alpha (0hpl, 83%; 1hpl, 105%; 6hpl, 93%; 12hpl, 112%; 24h, 76%; 48hpl, 112%; 72hpl, 111%; p>0.05; Fig. S2) showed no alteration in PPT compared to the respective time control.

An increase of NAPE-PLD protein amount was observed in DG from 1hpl to 6hpl (0hpl, 97%; p>0.05; 1hpl, 140%; 6hpl, 133%; p<0.05; Fig. 3). Thereafter, NAPE-PLD protein decreased to control levels (12hpl, 133%; 24h, 118%; 48hpl, 117%; 72hpl, 99%; p>0.05). The FAAH protein amount remained close to control levels up to 24hpl (1hpl, 110%; 6hpl, 108%; 12hpl, 106%;

24hpl, 111%; p>0.05). At 48hpl (120%; p<0.05) a significant peak of FAAH was observed that was no more visible at 72hpl (113%; p>0.05; Fig. 3). No change in the NAAA enzyme was detectable after dendritic denervation in the DG (1hpl 101%, 6hpl 98%, 12hpl 95%, 24h 128%, 48hpl 105%, 72hpl 111%, Fig. S2). The protein amount of CB_1 did not differ from the time control (0hpl, 119%; 1hpl, 101%; 6hpl, 77%; 12hpl, 107%; 24h, 123%; 48hpl, 105%; 72hpl, 109%; p>0.05, Fig. 3). The PPAR alpha protein amount did not change in comparison to the time controls (1hpl 102%, 6hpl 107%, 12hpl 114%, 24h 87%, 48hpl 107%, 72hpl 92%, p>0.05, Fig. S2).

In the CA1 region no alterations in NAPE-PLD were detected (0hpl, 89%; 1hpl, 100%; 6hpl, 112%; 12hpl, 109%; 24h, 86%; 48hpl, 100%; 72hpl, 86%; p>0.05; Fig. 3). FAAH (0hpl, 111%; 1hpl, 100%; 6hpl, 97%; 12hpl, 114%; 24h, 94%; 48hpl, 87%; 72hpl, 102%; p>0.05; Fig. 3) and NAAA (0hpl, 111%; 1hpl, 105%; 6hpl, 107%; 12hpl, 102%; 24h, 99%; 48hpl, 106%; 72hpl, 81%; p>0.05; Fig. S2) remained unchanged after PPT. In PPT CB_1 (0hpl, 93%; 1hpl, 106%; 6hpl, 87%; 12hpl, 94%; 24h, 99%; 48hpl, 126%; 72hpl, 82%; p>0.05; Fig. 3) as well as PPAR alpha
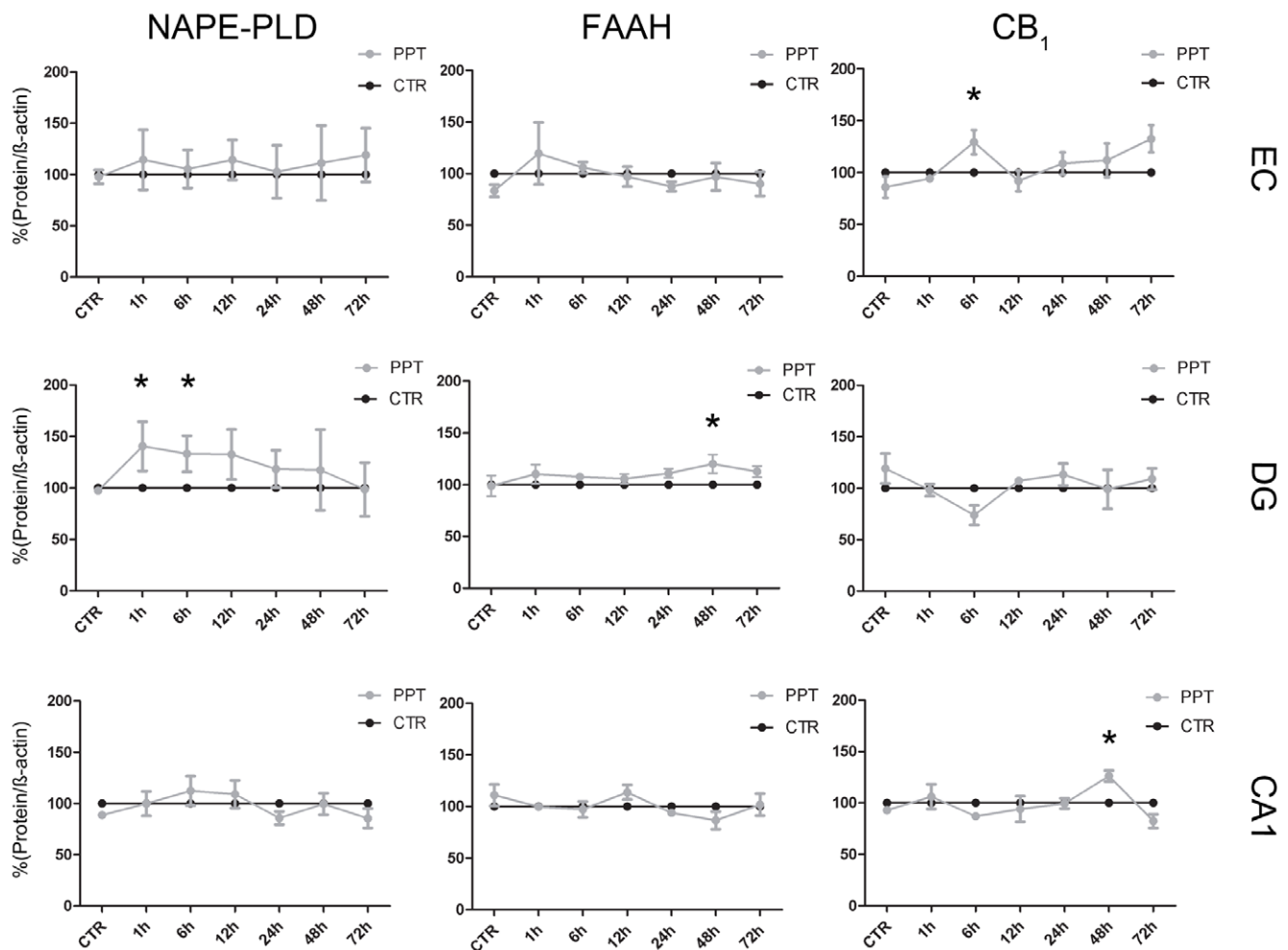
Figure 3. Relative amount of NAPE-PLD, FAAH and CB$_1$ after PPT as compared to respective time control (CTR) that were set as 100%. Whereas NAPE-PLD and FAAH remained constant after PPT in EC, the amount of CB$_1$ protein was significantly elevated 6hpl. In DG, NAPE-PLD was increased 1 and 6hpl. FAAH showed elevated levels 48hpl whereas CB$_1$ did not show any alteration after PPT. In CA1, NAPE-PLD and FAAH remained unchanged after PPT. In contrast, CB$_1$ levels were increased 48hpl. (n = 4, *p<0.05).
doi:10.1371/journal.pone.0033537.g003

(0hpl, 86%; 1hpl, 97%; 6hpl, 135%; 12hpl, 110%; 24 h, 97%; 48hpl, 124%; 72hpl, 69%; p>0.05; Fig. S2) were not altered after PPT in CA1 as compared to the respective time controls.

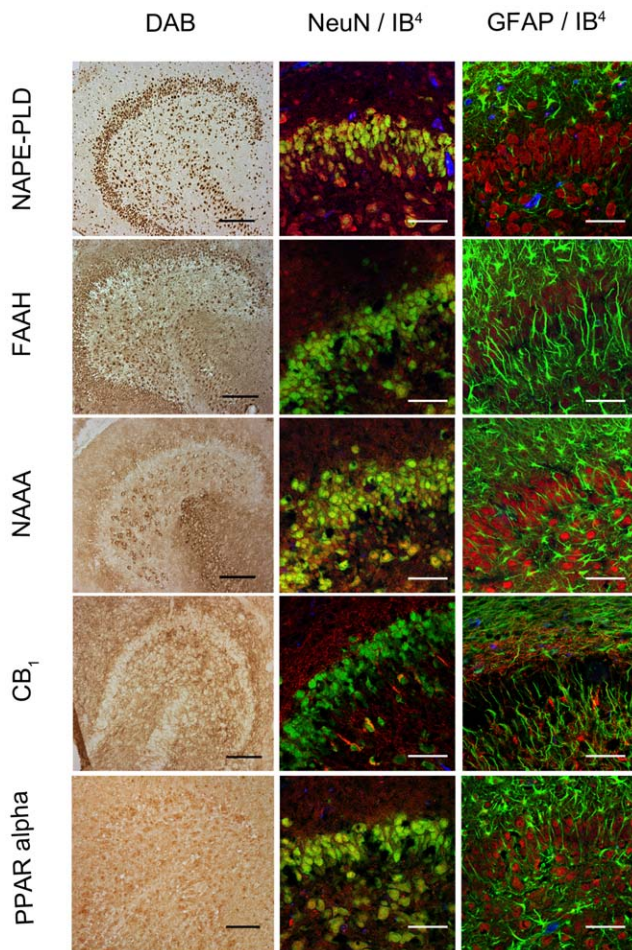## Distribution of NAPE-PLD, FAAH, NAAA, CB1 and PPAR alpha in OHSC

Localizations of NAPE-PLD, FAAH, NAAA, CB$_1$ and PPAR alpha immunoreactions were investigated in situ by immunohistochemical staining with NeuN, GFAP and IB$_4$ in sections obtained from OHSC at 24hpl. NAPE-PLD immunoreaction was found being co-localized with NeuN positive neurons and to a subset of IB$_4$ positive microglia. GFAP positive astrocytes did not show a NAPE-PLD immunoreaction (Fig. 4). FAAH immunoreactions showed a robust cytoplasmic distribution in neuronal cells. Neither microglial cells nor GFAP positive astrocytes exhibited a detectable amount of FAAH (Fig. 4). Co-localization of NAAA immunoreaction with NeuN positive neurons were observed, mainly in the perikarya. In addition some nuclei showed positive immunoreactions for NAAA. There was no overlap of NAAA immunoreaction with IB$_4$ or GFAP positive cells (Fig. 4). A strong CB$_1$ immunosignal was detected in the inner and outer molecular layer of the DG. CB$_1$ was present in some morphologically

characterized inter-neurons of the hilus. Whereas IB$_4$ positive microglia displayed a positive immunosignal for CB$_1$ this reaction was weak when GFAP immunoreactive astrocytes were examined (Fig. 4). PPAR alpha was found in NeuN immunoreactive neurons, IB$_4$ positive microglia and GFAP positive astrocytes. PPAR alpha was localized in vesicular structures close to the cell nucleus, apparently reflecting the Golgi apperatus throughout the entire OHSC.

Cellular distribution of NAPE-PLD, FAAH, NAAA, CB$_1$ and PPAR alpha in neurons, microglia and astrocytes

In isolated primary neuronal cell cultures NAPE-PLD immunoreaction was observed within neuronal perikarya and processes. Similar to OHSC, NAPE-PLD was found close to the nuclei in microglial cells. In primary astrocyte culture fibrillary astrocytes displayed a weak, protoplasmic astrocytes a robust NAPE-PLD immunoreaction (Fig. 5). Primary neurons, microglia and astrocytes showed a FAAH immunoreaction that was localized close to the nuclei, respectively (Fig. 5). An additional nuclear labeling was observed in microglia and astrocytes. Isolated primary neurons showed a NAAA immunoreaction that was found distributed in the perikarya and the secondary branches. Microglia was also labeled
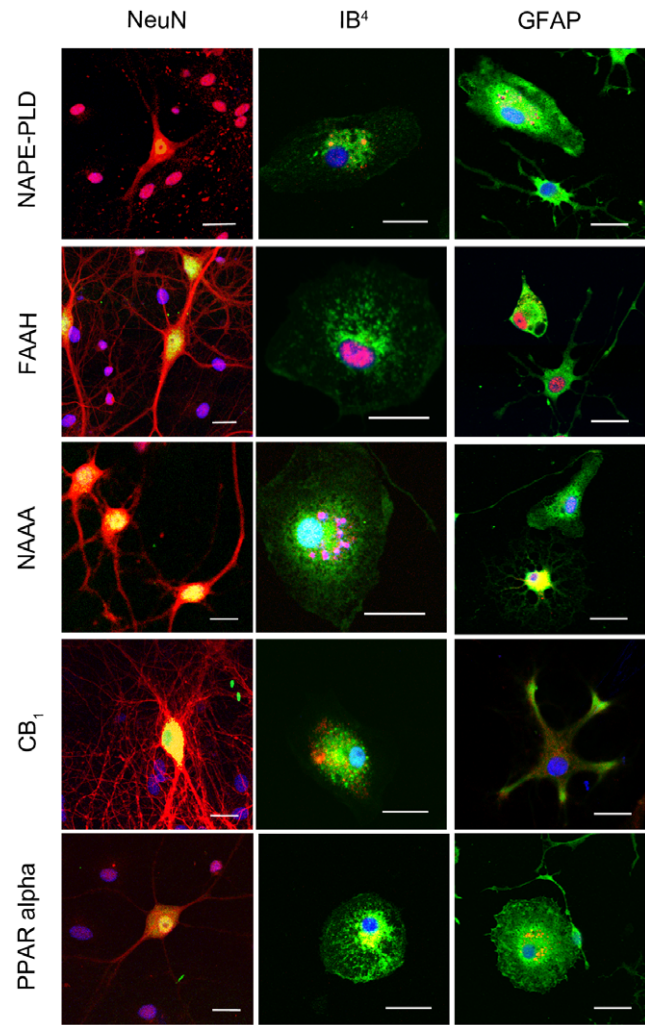
Figure 4. Immunocytochemical analyses of NAPE-PLD, FAAH, NAAA, CB₁ and PPAR alpha in dentate gyrus 24hpl. Left column: DG in overview after DAB staining. Middle column; Triple staining of eCB system related proteins with NeuN and IB₄. Right column; Triple staining of OHSC with eCB system related proteins in combination with NeuN and GFAP. The granular cell layer of the DG and interneurons in the hilus region showed a strong immunoreaction for NAPE-PLD. No overlap was observed with GFAP or IB₄. The granular cell layer of the DG and especially interneurons in the hilus region were strongly immunoreactive for FAAH. No overlap was observed with GFAP or IB₄. Please note the similarity of staining pattern of NAPE-PLD and FAAH immunoreactions. NAAA was found in perikarya and nuclei of neurons. In addition to granular cell layer of the DG and hilar neurons CA3 region was strongly labeled. Astrocytes and microglia seem free of NAAA. The entire molecular layer of the dentate gyrus showed a positive CB₁ immunoreaction. CB₁ was present in Microglia and to a lesser extent in astrocytes. PPAR alpha was observed in perikarya and nuclei of neurons. Microglia and Astrocytes showed a positive immunoreaction for PPAR alpha (n = 3, bars: left column = 100 μm, middle and right columns = 50 μm).
doi:10.1371/journal.pone.0033537.g004

with the NAAA antibody. Fibrillary astrocytes displayed NAAA immunoreactions within their cell bodies and to a minor extent in their processes (Fig. 5). Neurons showed a strong CB₁ immunoreaction in perikarya, primary and secondary neuronal processes and spines. Microglia and astrocytes demonstrated a CB₁ immunoreaction, although the immunoreaction in astrocytes was very weak (Fig. 5). PPAR alpha immunoreaction was detectable in primary neurons, microglia and astrocytes (Fig. 5). In neurons PPAR alpha was scattered over the entire perikarya, whereas in glial cells it was found close to the nuclei, respectively.

Figure 5. Immunocytochemical analyses of NAPE-PLD, FAAH, NAAA, CB₁ and PPAR alpha in primary neuronal (left column), microglia (middle column) and astrocyte (left column) cell cultures. In neurons, NAPE-PLD was distributed in the perikarya but not in neuronal processes. In microglia NAPE-PLD immunoreactions was detectable in small vesicles closely located to the nucleus. NAPE-PLD was not found in protoplasmic astrocytes whereas fibrillary astrocytes showed an immunosignal comparable to microglia. The immunosignal for FAAH in primary neurons was localized in the cell bodies as well as in the primary branches of the neurites. In microglia and astrocytes, FAAH was localized within the nucleus, respectively. In fibrillary astrocytes a FAAH immunoreaction was additionally observed in vesicles. NAAA was clearly found in neurons but was barely found in microglia and astrocytes. In microglia NAAA showed a vesicular staining pattern close to the nucleus. Protoplasmic astrocytes were immunoreactive for NAAA whereas fibrillary astrocytes did not show any NAAA immunosignal. A robust CB₁ immunoreaction was found in neurons. To a lower extent, CB₁ immunosignals were detectable in microglia and astrocytes. Primary neurons showed a strong PPAR alpha immunoreaction in their Perikarya and nuclei. Microglia and astrocytes were positive for PPAR alpha immunoreaction in a vesicular pattern. (n = 3, bar = 20 μm).
doi:10.1371/journal.pone.0033537.g005

Discussion

Widespread secondary neurodegeneration occurs in the CNS after traumatic brain injury (TBI), spinal cord injury (SCI) and other CNS pathologies involving lesion of long-range projections. Recent studies demonstrated the neuroprotective properties of

eCBs in various models of neuronal lesion in vitro and in vivo. It is well accepted that the eCB system represents a major modulator of synaptic transmission e.g. the ability of eCB to counteract excitotoxicity by reducing the calcium influx in excitatory glutamatergic neurons [26,27]. In previous studies we found a strong variation between different cannabinoids with regard to their efficacy to prevent excitotoxic neuronal injury and to their mode of action on neuroprotection. Whereas AEA and the phytocannabinoid THC failed to protect dentate gyrus neurons, PEA as well as the endocannabinoids NADA and 2-AG and the synthetically designed cannabinoid WIN 55–212, 2 clearly showed neuroprotective effects. While CB_1 receptor activation was responsible for WIN 55–212, 2 and NADA-mediated neuroprotection, PEA mediated its neuroprotective effects via dual PPAR alpha activation on microglial cells and neurons. Finally 2-AG was shown to activate abn-CBD receptors on microglial cells to mediate its neuroprotective effects [27,28,29,30,31].

Since some modes of action of eCB during detrimental processes in the brain are well understood, very little is known about the intrinsic regulation of the eCB system after transection of long-range projections in origin and target areas. Thus, by using the PPT model in OHSC the present study has been designed to investigate the intrinsic regulation of eCBs after lesion of long-range projections. This model, well known and highly accepted, allows a clear differentiation between anterograde, retrograde and more distant area changes induced by axonal injury. It should be considered that slice cultures derived from young animals show spontaneous seizure like events when investigated shortly after dissection [32] but these events disappear when cultures are kept in vitro for 7–21 days [33,34,35]. The activation of endocannabinoid system during the course of status epilepticus has very recently been reported in humans [36]. In the present investigation we didn't have noticed elevated endocannabinoid values under control conditions. Furthermore, the PPT group has always been analyzed in comparison to time match controls suggesting that changes in the amount of eCBS are most likely due to perforant pathway transection rather than an increase by spontaneous seizure like events.

The combination of the PPT model with the precise dissection of differentially linked regions forms a highly convenient model allowing profound insights in intrinsic regulation of eCB system after long-range projection damage.

We first examined neuronal cell death after PPT in OHSC and found that after 1, 6, 12, 24, 48, and 72hpl no significant changes in the number of PI^+ neuronal nuclei was observed when compared to unlesioned control OHSC. These findings are in accordance with previous reports showing almost no neurodegeneration after PPT in dentate gyrus [19]. We then precisely dissected the specific areas, namely entorhinal cortex (EC), dentate gyrus (DG) and cornu ammonis 1 region (CA1) in controls and after PPT and investigated the regulation of AEA, PEA and OEA.

Small but not significant changes were observed in the EC, whereas a significant and robust increase in the concentration of all three eCBs investigated was found 24hpl in the DG. In the CA1 region a decrease of PEA and OEA but not AEA was seen after 12 and 48hpl. These findings indicate a spatial and temporal regulation of NEA mostly affecting the target area of long-range projections. Little is known about the specific regulation of NEA after transecion of long-range projections. In several reports enhanced AEA levels have been detected after various pathological events indicating a compensatory mechanism to brain damage [37,38,39]. In human studies, elevated AEA levels were measured in the cerebrospinal fluids of patients with Parkinson disease or after stroke and the increase in AEA was directly associated with

brain damage [40,41]. With regard to long-range projections, our data now asks for an additional consideration of more distant areas than the PPT, e.g. denervated spinal cord neurons as a source for AEA production to concern the regulation of eCB after transaction of long-range somato-afferent and/or efferent projections.

As a known CB_1 agonist AEA activates at cellular level mitogen-activated protein kinase phosphatase-1 (MKP-1) decreasing MAPK signal transduction in microglial cells abolishing NO release and protects against over-activation of microglia [42,43]. Therefore, the increase of AEA levels 24hpl in our study might reduce the microglia activation leading to neuroprotective effects. Stella and his group found in BV-2 cells an increase in microglia motility by AEA [44]. Similar to AEA, increased PEA levels observed here at 24hpl were also measured in inflamed tissues undergoing severe cell damaging processes, ischemic conditions and glutamate induced neurotoxicity and demonstrated neuroprotective properties [27,45,46]. One underlying mechanism seems an enhanced action of AEA on the vanilloid receptor caused by increased PEA levels, the so called entourage effect [47]. Further, PEA is reported to protect neurons via activation of PPAR alpha in neurons, microglia [27] and astrocytes [48]. OEA is suggested as a modulator of satiety, inflammation, lipid metabolism and antinociceptive effects, due to its activity at receptors such as TRPV1, GPR119 or PPAR gamma [46,49,50,51]. The increase of OEA at 24hpl in the present study go along with a study of Galan-Rotriguez, demonstrating neuroprotective effects of OEA in dopamine neurons in the substantia nigra after 6-OHDA treatment [52]. Enhanced OEA levels were found to reduce microglia activation [53,54]. Inhibition of reactive microglia by OEA might explain the lack of neurodegeneration after PPT in our system.

The diverse regulation of NEA in different brain regions after PPT demonstrates a specific involvement of eCBs in distinct damage regulation in the brain. Whether NEA perform different tasks or are separately regulated or act orchestral after PPT needs further investigation. Hansen et al. mentioned the difficulty of PEA and OEA data interpretation due to their structural similarity and comparable regulation to anandamide [55].

As a next step we investigated the time-dependent and spatial regulation of enzymes responsible for synthesis and hydrolysis of the NEAs. NAPE-PLD, synthesizing NEA from NAPE [13,56], was elevated early between 1hpl and 6hpl after PPT but decreased to control levels at 72hpl. This time course of NAPE-PLD might explain the NEA elevation. A recent study showed a tight relation between regulation of NAPE-PLD and PEA levels and its impact on cell functions. It was shown that LPS decreased NAPE-PLD protein amount in macrophage cell cultures, leading to decreased PEA levels which finally led to subsequently exacerbated inflammatory reactions [57]. Interestingly, mice lacking NAPE-PLD did not exhibit lowered PEA levels [57]. It was assumed that two further synthesizing pathways compensate the lack of NAPE-PLD and take over NEA synthesis: (1) phospholipase C (PLC) creates a phosphor-NEA that is further catabolized by a phosphatase to NEA or, (2) via a combined action of a phospholipase B (Abh4) and a phosphodiesterase (GDE1) that hydrolyzes glycerophospho-NAE (GP-NAE) [58,59]. It remained unclear whether these additional pathways are functionally activated in the presence of NAPE-PLD or were compensatory upregulated as well whether these alternative pathways are also involved in NEA synthesis after PPT.

Whereas FAAH was found being predominantly localized in endoplasmic reticulum [14] and able to hydrolyze all three here investigated acylethanolamides [16], NAE-hydrolyzing acid ami-

dase (NAAA) detected in lysosomes [60] is responsible for the hydrolysis of acylethanolamides of less than 18 carbon atoms, a group of NEAs to which PEA significantly belongs to. FAAH was up-regulated at 48hpl, whereas NAAA protein remained unchanged at any time points after PPT. The up-regulation of FAAH was supposed to be responsible for the down-regulation of the NEA found at 48hpl. Evidence exists that reduction in NEA level by FAAH correlated with neurotoxic properties, as the FAAH inhibitor MAFP reduced apoptosis in the neocortex [61] or the inhibitor URB 597 decreased the infarct volume when administered before the focal cerebral ischemia [62]. Also other FAAH inhibitors were found to be beneficial for the outcome of neurological diseases [63]. Further investigations are required to figure out whether the here observed endogenous up-regulation of FAAH display the natural end of the inflammatory reaction or is directly involved in protective/harming effects.

Though, the enzymatic machinery for biosynthesis and catabolism of eCB is strongly affected by PPT in DG and CA1, we only found a variation for a potential target receptor of AEA, namely CB_1 in the EC. This is in line with findings showing that middle cerebral artery occlusion in rats enhanced CB_1 expression from 2 h on that persisted for 72 h in the ischemic region only [64]. The effects of ischemic insults upon CB_1, however, is unclear and seems to depend from ischemic condition, time and species investigated [63]. Studies of differential regulated CB_1 receptors on glutamatergic and GABAergic synapses might clarify these coherences [38]. A nuclear receptor for NEA is PPAR alpha [49,65]. Application of exogenous PEA was reported to enhance PPAR alpha activation. Furthermore, selective NAAA inhibitors were reported to up-regulate the endogenous PEA levels and subsequently increase PPAR alpha activity [66,67].

To clarify the protein regulation responsible for the observed NEA levels, cellular distribution of NAPE-PLD, FAAH, NAAA, CB_1 and PPAR alpha were investigated by immunohistochemistry. A clear neuronal distribution in primary neurons as well as in OHSC was observed for NAPE-PLD and corresponded to previously described results [68]. NAPE-PLD was found in primary cultures of both microglia and astrocytes, however only microglia was immunoreactive in OHSC. In strongly inflamed postmortem brain specimens of MS patients NAPE-PLD immunoreactive microglia and astrocytes were observed [69]. FAAH clearly showed a neuronal distribution as previously reported by Cravatt et al. [14]. In OHSC FAAH was not seen in microglia neither in PPT nor in controls whereas primary microglia cell cultures expressed FAAH as shown in literature [70,71]. In accordance to previous reports in Alzheimer disease we found in primary cell cultures, low FAAH expression in fibrillary and high FAAH expression in protoplasmic astrocytes [72]. To our knowledge, we showed here for the first time a clear neuronal NAAA distribution. NAAA was absent in IB_4 and in GFAP positive cells in OHSC but was surprisingly present in primary cell cultures. So far, NAAA was solely described in macrophages as a lysosome associated protein [16]. Moreover, fibrillary astrocytes also showed high NAAA expression whereas protoplasmic astrocytes displayed weak NAAA in their nuclei only. In general the discrepancies between the findings especially for microglial cells regarding NAPE-PLD, FAAH and NAAA expression in primary cell cultures and complex OHSC

might be due to the activation state of microglia in isolated cell cultures and the lack of factors present in CNS milieu. No obvious change over time was observed in histological staining with CB_1. The potency of glial cells to synthesize and catabolize NEA under physiological or pathological conditions represents the high flexibility and complexity of the eCB system. Primary cultures displayed a different picture of enzyme and receptor distribution as in the complex model of OHSC. We therefore can state that in OHSC neurons and microglia produce NEA whereas hydrolysis of NEAs mainly happens in neurons. Depending on the lesion paradigm the machinery for production and degradation of NEA can be up-regulated in astrocytes as well.

Taken together the activation of the eCB system after neuronal damage by transection of long-range projections apparently provides a strong time-dependent and area confined signal for de novo synthesis of eCB, presumably to prevent or restrict neuronal damage. The present data underlines the importance of eCB in CNS pathologies and identified a site-specific intrinsic regulation of eCB levels in long-range projection damage. The highly dynamic eCB system represents an intrinsic, presumably protective system in the CNS.

Supporting Information

Figure S1 Specificity test for antibodies. A: Specificity test for antibodies against NAPE-PLD, FAAH, NAAA and PPAR alpha by Western blot analyses. The antibody against NAPE-PLD showed two immunoreactive bands of about 46 kDa (1). Both bands were blocked by use of the respective blocking peptide (2). Similar to NAPE-PLD immunoreactive bands for FAAH, NAAA and PPAR alpha disappeared after preabsorption with respective peptides. B: NAPE-PLD, FAAH and NAAA fluorescent staining after preincubation of sections with respective blocking peptides or CB_1 fluorescent staining in sections derived from CB_1 knock out animals (Bar = 50 μm).
(TIF)

Figure S2 Time-dependent regulation of NAAA and PPAR alpha in OHSC. The data was shown in relation to the matching time controls that were set as 100%. In all regions investigated (EC, DG and CA1) no significant difference was found in OHSC after PPT as compared to controls (CTR).
(TIF)

Author Contributions

Conceived and designed the experiments: GG MK FD. Performed the experiments: SK CH AE SZ MK. Analyzed the data: SK SZ MK FD. Contributed reagents/materials/analysis tools: NU GG. Wrote the paper: SK MK FD.

References

1. Signoretti S, Vagnozzi R, Tavazzi B, Lazzarino G (2010) Biochemical and neurochemical sequelae following mild traumatic brain injury: summary of experimental data and clinical implications. Neurosurg Focus 29: E1.
2. Dirnagl U, Iadecola C, Moskowitz MA (1999) Pathobiology of ischaemic stroke: an integrated view. Trends Neurosci 22: 391–397.
3. Yakovlev AG, Faden AI (2004) Mechanisms of neural cell death: implications for development of neuroprotective treatment strategies. NeuroRx 1: 5–16.
4. Faden AI, Stoica B (2007) Neuroprotection: challenges and opportunities. Arch Neurol 64: 794–800.
5. Dumont RJ, Okonkwo DO, Verma S, Hurlbert RJ, Boulos PT, et al. (2001) Acute spinal cord injury, part I: pathophysiologic mechanisms. Clin Neuropharmacol 24: 254–264.
6. Piomelli D (2003) The molecular logic of endocannabinoid signalling. Nat Rev Neurosci 4: 873–884.

7. Howlett AC, Barth F, Bonner TI, Cabral G, Casellas P, et al. (2002) International Union of Pharmacology. XXVII. Classification of cannabinoid receptors. Pharmacol Rev 54: 161–202.

8. Matsuda LA, Lolait SJ, Brownstein MJ, Young AC, Bonner TI (1990) Structure of a cannabinoid receptor and functional expression of the cloned cDNA. Nature 346: 561–564.

9. Pertwee RG, Howlett AC, Abood ME, Alexander SP, Di Marzo V, et al. (2010) International Union of Basic and Clinical Pharmacology. LXXIX. Cannabinoid receptors and their ligands: beyond CB and CB. Pharmacol Rev 62: 588–631.

10. Devane WA, Hanus L, Breuer A, Pertwee RG, Stevenson LA, et al. (1992) Isolation and structure of a brain constituent that binds to the cannabinoid receptor. Science 258: 1946–1949.

11. Sugiura T, Kondo S, Sukagawa A, Nakane S, Shinoda A, et al. (1995) 2-Arachidonoylglycerol: a possible endogenous cannabinoid receptor ligand in brain. Biochem Biophys Res Commun 215: 89–97.

12. Pertwee RG (2010) Receptors and channels targeted by synthetic cannabinoid receptor agonists and antagonists. Curr Med Chem 17: 1360–1381.

13. Okamoto Y, Morishita J, Tsuboi K, Tonai T, Ueda N (2004) Molecular characterization of a phospholipase D generating anandamide and its congeners. J Biol Chem 279: 5298–5305.

14. Cravatt BF, Giang DK, Mayfield SP, Boger DL, Lerner RA, et al. (1996) Molecular characterization of an enzyme that degrades neuromodulatory fatty-acid amides. Nature 384: 83–87.

15. Ueda N (2002) Endocannabinoid hydrolases. Prostaglandins Other Lipid Mediat 68–69: 521–534.

16. Ueda N, Tsuboi K, Uyama T (2010) N-acylethanolamine metabolism with special reference to N-acylethanolamine-hydrolyzing acid amidase (NAAA). Prog Lipid Res 49: 299–315.

17. Deller T (1997) The anatomy of the rat fascia dentata–new vistas. Ann Anat 179: 501–504.

18. Frotscher M, Heimrich B, Deller T (1997) Sprouting in the hippocampus is layer-specific. Trends Neurosci 20: 218–223.

19. Kovac AD, Kwidzinski E, Heimrich B, Bittigau P, Deller T, et al. (2004) Entorhinal cortex lesion in the mouse induces transsynaptic death of perforant path target neurons. Brain Pathol 14: 249–257.

20. Stoppini L, Buchs PA, Muller D (1991) A simple method for organotypic cultures of nervous tissue. J Neurosci Methods 37: 173–182.

21. Ramirez JJ (2001) The role of axonal sprouting in functional reorganization after CNS injury: lessons from the hippocampal formation. Restor Neurol Neurosci 19: 237–262.

22. Brewer GJ, Torricelli JR, Evege EK, Price PJ (1993) Optimized survival of hippocampal neurons in B27-supplemented Neurobasal, a new serum-free medium combination. J Neurosci Res 35: 567–576.

23. Deller T, Del Turco D, Rappert A, Bechmann I (2007) Structural reorganization of the dentate gyrus following entorhinal denervation: species differences between rat and mouse. Prog Brain Res 163: 501–528.

24. Bishay P, Schmidt H, Marian C, Haussler A, Wijnvoord N, et al. (2010) R-flurbiprofen reduces neuropathic pain in rodents by restoring endogenous cannabinoids. PLoS One 5: e10628.

25. Tsuboi K, Zhao LY, Okamoto Y, Araki N, Ueno M, et al. (2007) Predominant expression of lysosomal N-acylethanolamine-hydrolyzing acid amidase in macrophages revealed by immunochemical studies. Biochim Biophys Acta 1771: 623–632.

26. Zhao Y, Yuan Z, Liu Y, Xue J, Tian Y, et al. (2010) Activation of cannabinoid CB2 receptor ameliorates atherosclerosis associated with suppression of adhesion molecules. J Cardiovasc Pharmacol 55: 292–298.

27. Koch M, Kreutz S, Bottger C, Benz A, Maronde E, et al. (2011) Palmitoylethanolamide protects dentate gyrus granule cells via peroxisome proliferator-activated receptor-alpha. Neurotox Res 19: 330–340.

28. Kreutz S, Koch M, Ghadban C, Korf HW, Dehghani F (2007) Cannabinoids and neuronal damage: differential effects of THC, AEA and 2-AG on activated microglial cells and degenerating neurons in excitotoxically lesioned rat organotypic hippocampal slice cultures. Exp Neurol 203: 246–257.

29. Kreutz S, Koch M, Bottger C, Ghadban C, Korf HW, et al. (2009) 2-Arachidonoylglycerol elicits neuroprotective effects on excitotoxically lesioned dentate gyrus granule cells via abnormal-cannabidiol-sensitive receptors on microglial cells. Glia 57: 286–294.

30. Grabiec U, Koch M, Kallendrusch S, Kraft R, Hill K, et al. (2011) The endocannabinoid N-arachidonoyldopamine (NADA) exerts neuroprotective effects after excitotoxic neuronal damage via cannabinoid receptor 1 (CB(1)). Neuropharmacology.

31. Koch M, Kreutz S, Bottger C, Grabiec U, Ghadban C, et al. (2011) The cannabinoid WIN 55,212-2-mediated protection of dentate gyrus granule cells is driven by CB1 receptors and modulated by TRPA1 and Ca(v) 2.2 channels. Hippocampus 21: 554–564.

32. Schuchmann S, Albrecht D, Heinemann U, von Bohlen und Halbach O (2002) Nitric oxide modulates low-Mg2+-induced epileptiform activity in rat hippocampal-entorhinal cortex slices. Neurobiol Dis 11: 96–105.

33. Kovacs R, Rabanus A, Otahal J, Patzak A, Kardos J, et al. (2009) Endogenous nitric oxide is a key promoting factor for initiation of seizure-like events in hippocampal and entorhinal cortex slices. J Neurosci 29: 8565–8577.

34. Ziobro JM, Deshpande LS, Delorenzo RJ (2011) An organotypic hippocampal slice culture model of excitotoxic injury induced spontaneous recurrent epileptiform discharges. Brain Res 1371: 110–120.

35. Bhaskaran MD, Smith BN (2010) Cannabinoid-mediated inhibition of recurrent excitatory circuitry in the dentate gyrus in a mouse model of temporal lobe epilepsy. PLoS One 5: e10683.

36. Goffin K, Van Paesschen W, Van Laere K (2011) In vivo activation of endocannabinoid system in temporal lobe epilepsy with hippocampal sclerosis. Brain 134: 1033–1040.

37. Hansen HH, Schmid PC, Bittigau P, Lastres-Becker I, Berrendero F, et al. (2001) Anandamide, but not 2-arachidonoylglycerol, accumulates during in vivo neurodegeneration. J Neurochem 78: 1415–1427.

38. Marsicano G, Goodenough S, Monory K, Hermann H, Eder M, et al. (2003) CB1 cannabinoid receptors and on-demand defense against excitotoxicity. Science 302: 84–88.

39. Maccarrone M, Gubellini P, Bari M, Picconi B, Battista N, et al. (2003) Levodopa treatment reverses endocannabinoid system abnormalities in experimental parkinsonism. J Neurochem 85: 1018–1025.

40. Schabitz WR, Giuffrida A, Berger C, Aschoff A, Schwaninger M, et al. (2002) Release of fatty acid amides in a patient with hemispheric stroke: a microdialysis study. Stroke 33: 2112–2114.

41. Pisani A, Fezza F, Galati S, Battista N, Napolitano S, et al. (2005) High endogenous cannabinoid levels in the cerebrospinal fluid of untreated Parkinson's disease patients. Ann Neurol 57: 777–779.

42. Eljaschewitsch E, Witting A, Mawrin C, Lee T, Schmidt PM, et al. (2006) The endocannabinoid anandamide protects neurons during CNS inflammation by induction of MKP-1 in microglial cells. Neuron 49: 67–79.

43. Dommergues MA, Plaisant F, Verney C, Gressens P (2003) Early microglial activation following neonatal excitotoxic brain damage in mice: a potential target for neuroprotection. Neuroscience 121: 619–628.

44. Franklin A, Parmentier-Batteur S, Walter L, Greenberg DA, Stella N (2003) Palmitoylethanolamide increases after focal cerebral ischemia and potentiates microglial cell motility. J Neurosci 23: 7767–7775.

45. Conti S, Costa B, Colleoni M, Parolaro D, Giagnoni G (2002) Antiinflammatory action of endocannabinoid palmitoylethanolamide and the synthetic cannabinoid nabilone in a model of acute inflammation in the rat. Br J Pharmacol 135: 181–187.

46. Rodriguez De Fonseca F, Gorriti MA, Bilbao A, Escuredo L, Garcia-Segura LM, et al. (2001) Role of the endogenous cannabinoid system as a modulator of dopamine transmission: implications for Parkinson's disease and schizophrenia. Neurotox Res 3: 23–35.

47. De Petrocellis L, Davis JB, Di Marzo V (2001) Palmitoylethanolamide enhances anandamide stimulation of human vanilloid VR1 receptors. FEBS Lett 506: 253–256.

48. Raso GM, Esposito E, Vitiello S, Iacono A, Santoro A, et al. (2011) Palmitoylethanolamide stimulation induces allopregnanolone synthesis in C6 Cells and primary astrocytes: involvement of peroxisome-proliferator activated receptor-alpha. J Neuroendocrinol 23: 591–600.

49. Suardiaz M, Estivill-Torrus G, Goicoechea C, Bilbao A, Rodriguez de Fonseca F (2007) Analgesic properties of oleoylethanolamide (OEA) in visceral and inflammatory pain. Pain 133: 99–110.

50. Fu J, Gaetani S, Oveisi F, Lo Verme J, Serrano A, et al. (2003) Oleylethanolamide regulates feeding and body weight through activation of the nuclear receptor PPAR-alpha. Nature 425: 90–93.

51. Thabuis C, Tissot-Favre D, Bezelgues JB, Martin JC, Cruz-Hernandez C, et al. (2008) Biological functions and metabolism of oleoylethanolamide. Lipids 43: 887–894.

52. Galan-Rodriguez B, Suarez J, Gonzalez-Aparicio R, Bermudez-Silva FJ, Maldonado R, et al. (2009) Oleoylethanolamide exerts partial and dose-dependent neuroprotection of substantia nigra dopamine neurons. Neuropharmacology 56: 653–664.

53. Coffey PJ, Perry VH, Rawlins JN (1990) An investigation into the early stages of the inflammatory response following ibotenic acid-induced neuronal degeneration. Neuroscience 35: 121–132.

54. Topper R, Gehrmann J, Schwarz M, Block F, Noth J, et al. (1993) Remote microglial activation in the quinolinic acid model of Huntington's disease. Exp Neurol 123: 271–283.

55. Hansen HS (2010) Palmitoylethanolamide and other anandamide congeners. Proposed role in the diseased brain. Exp Neurol 224: 48–55.

56. Leung D, Saghatelian A, Simon GM, Cravatt BF (2006) Inactivation of N-acyl phosphatidylethanolamine phospholipase D reveals multiple mechanisms for the biosynthesis of endocannabinoids. Biochemistry 45: 4720–4726.

57. Zhu C, Solorzano C, Sahar S, Realini N, Fung E, et al. (2011) Proinflammatory stimuli control N-acylphosphatidylethanolamine-specific phospholipase D expression in macrophages. Mol Pharmacol 79: 786–792.

58. Sun YX, Tsuboi K, Okamoto Y, Tonai T, Murakami M, et al. (2004) Biosynthesis of anandamide and N-palmitoylethanolamine by sequential actions of phospholipase A2 and lysophospholipase D. Biochem J 380: 749–756.

59. Simon GM, Cravatt BF (2008) Anandamide biosynthesis catalyzed by the phosphodiesterase GDE1 and detection of glycerophospho-N-acyl ethanolamine precursors in mouse brain. J Biol Chem 283: 9341–9349.

60. Zhao LY, Tsuboi K, Okamoto Y, Nagahata S, Ueda N (2007) Proteolytic activation and glycosylation of N-acylethanolamine-hydrolyzing acid amidase, a lysosomal enzyme involved in the endocannabinoid metabolism. Biochim Biophys Acta 1771: 1397–1405.

61. Maccarrone M, Piccirilli S, Battista N, Del Duca C, Nappi G, et al. (2004) Enhanced anandamide degradation is associated with neuronal apoptosis

induced by the HIV-1 coat glycoprotein gp120 in the rat neocortex. J Neurochem 89: 1293–1300.

62. Degn M, Lambertsen KL, Petersen G, Meldgaard M, Artmann A, et al. (2007) Changes in brain levels of N-acylethanolamines and 2-arachidonoylglycerol in focal cerebral ischemia in mice. J Neurochem 103: 1907–1916.

63. Fowler CJ, Rojo ML, Rodriguez-Gaztelumendi A (2010) Modulation of the endocannabinoid system: neuroprotection or neurotoxicity? Exp Neurol 224: 37–47.

64. Jin KL, Mao XO, Goldsmith PC, Greenberg DA (2000) CB1 cannabinoid receptor induction in experimental stroke. Ann Neurol 48: 257–261.

65. De Petrocellis L, Chu CJ, Moriello AS, Kellner JC, Walker JM, et al. (2004) Actions of two naturally occurring saturated N-acyldopamines on transient receptor potential vanilloid 1 (TRPV1) channels. Br J Pharmacol 143: 251–256.

66. Lo Verme J, Fu J, Astarita G, La Rana G, Russo R, et al. (2005) The nuclear receptor peroxisome proliferator-activated receptor-alpha mediates the anti-inflammatory actions of palmitoylethanolamide. Mol Pharmacol 67: 15–19.

67. Solorzano C, Zhu C, Battista N, Astarita G, Lodola A, et al. (2009) Selective N-acylethanolamine-hydrolyzing acid amidase inhibition reveals a key role for

68. Nyilas R, Dudok B, Urban GM, Mackie K, Watanabe M, et al. (2008) Enzymatic machinery for endocannabinoid biosynthesis associated with calcium stores in glutamatergic axon terminals. J Neurosci 28: 1058–1063.

69. Zhang H, Hilton DA, Hanemann CO, Zajicek J (2011) Cannabinoid Receptor and N-acyl Phosphatidylethanolamine Phospholipase D-Evidence for Altered Expression in Multiple Sclerosis. Brain Pathol.

70. Witting A, Walter L, Wacker J, Moller T, Stella N (2004) P2X7 receptors control 2-arachidonoylglycerol production by microglial cells. Proc Natl Acad Sci U S A 101: 3214–3219.

71. Tham CS, Whitaker J, Luo L, Webb M (2007) Inhibition of microglial fatty acid amide hydrolase modulates LPS stimulated release of inflammatory mediators. FEBS Lett 581: 2899–2904.

72. Nunez E, Benito C, Tolon RM, Hillard CJ, Griffin WS, et al. (2008) Glial expression of cannabinoid CB(2) receptors and fatty acid amide hydrolase are beta amyloid-linked events in Down's syndrome. Neuroscience 151: 104–110.

endogenous palmitoylethanolamide in inflammation. Proc Natl Acad Sci U S A 106: 20966–20971.